# Enhancement of the Performance of Perovskite Solar Cells, LEDs, and Optical Amplifiers by Anti-Solvent Additive Deposition

*Thi Tuyen Ngo, Isaac Suarez, Gabriella Antonicelli, Diego Cortizo-Lacalle, Juan P. Martinez-Pastor,* Aurelio Mateo-Alonso,* and Ivan Mora-Sero**

Halide perovskites (PS) have emerged as an outstanding material family for optoelectronic applications[1] because of their superior physical properties, such as high optical absorption coefficients,[2] benign defect physics,[3] long and balanced electron–hole diffusion lengths,[4] good charge transport properties even in polycrystalline films,[1a] and low non-radiative recombination.[5] Photoconversion efficiency has reached 22.1%[6] a few years after the first reports on PS-based liquid electrolyte solar cells in 2009.[7] Besides the application in photovoltaics, PS have been successfully employed in light-emitting diodes (LEDs),[8] optical amplifiers,[9] and lasers.[10] In addition, the success of these materials mainly lies in that high-efficiency devices are prepared with PS polycrystalline films that can be grown using solution methods[5c,11] at low processing temperatures and, consequently, using low-cost fabrication techniques. Furthermore, these growth techniques allow the easy combination of PS with other materials, for example, PbS quantum dots,[12] that induce interesting synergies. This fact opens a broad range of possibilities for the interaction of PS with organic compounds beyond their use as selective contacts.[13] Organic compounds are appealing materials for electronic applications since an unlimited number of structures can be potentially synthesized and they are relatively easy to design and/or modify to meet the requirements of specific applications.

T. T. Ngo, Prof. I. Mora-Sero
Institute of Advanced Materials (INAM)
UniversitatJaume I
12006 Castelló, Spain
E-mail: sero@uji.es
Dr. I. Suarez, Prof. J. P. Martínez-Pastor
UMDO
Instituto de Ciencia de los Materiales
Universidad de Valencia
46071 Valencia, Spain
E-mail: Juan.Mtnez.Pastor@uv.es
G. Antonicelli, Dr. D. Cortizo-Lacalle,
Prof. A. Mateo-Alonso
POLYMAT
University of the Basque Country UPV/EHU
Avenida de Tolosa 72, E-20018 Donostia-San Sebastian, Spain
E-mail: amateo@polymat.eu
Prof. A. Mateo-Alonso
Ikerbasque
Basque Foundation for Science
E-48011 Bilbao, Spain

**DOI: 10.1002/adma.201604056**

The passivation of PS plays a crucial role in the efficiency of PS-based devices as it has been shown that the presence of electron traps favors faster non-radiative decays, while long carrier lifetimes and high photoluminescence (PL) efficiencies are in general indicators of better performing PS layers. Exposure of PS films to electron-deficient aromatic compounds such as pyridine[14] and [6,6]-phenyl-$C_{61}$-butyric acid methyl esther (PCBM)[15] have resulted in enhanced efficiencies associated to the passivation of such electron traps. Among the myriad of different electron-deficient aromatic compounds, nitrogen-containing polycyclic aromatic hydrocarbons (N-PAHs)[16] have recently reemerged as a platform for developing small molecule n-type semiconductors that have been able to compete with fullerenes in several applications.[17] In particular, N-PAHs containing pyrazine rings have attracted much attention as they combine a series of optimal optoelectronic and electric properties that can further be tuned thanks to the recent development of straightforward and solid synthetic routes.[16]

We have developed a new method to introduce additives in situ in a halide perovskite thin film, during the anti-solvent deposition step.[11b,c,18] Solar-cell, LED, and waveguide-optical-amplifier devices have been prepared using the perovskite layer, concretely $CH_3NH_3PbI_3$, mixed separately with two different electron-deficient heteroatom-doped PAHs, namely, a twisted hexaazatrinaphthylene (HATNA)[16i,19] and a bisthiadiazole-fused tetraazapentacenequinone (DCL97)[20] (**Figure 1**). We have selected these two compounds among others as: i) they are novel compounds with different functionalities that have not been previously checked for passivation in perovskite optoelectronic devices; ii) they contain PAHs that have been reported to be excellent passivation agents,[14,15] displaying electrochemical LUMOs (or electron affinities) in the range of those observed for fullerene derivatives with excellent results for passivation;[15] iii) they possess different but complementary electronic absorption spectra that allow the selective excitation for characterization purposes and also investigating if their absorption features might also play a role under illumination; and iv) they are soluble and chemically stable in the anti-solvents required for the fabrication of the devices.

With both molecules, we have observed a significant improvement of the performance of PS-based solar-cell, LED, and waveguide-optical-amplifier devices. Photoconversion efficiency of solar cells has been increased with respect to a reference cell, with no additives, while current/potential hysteresis decreased and solar-cell stability increased. We have also observed an increase of the external quantum efficiency (EQE) for PS LEDs

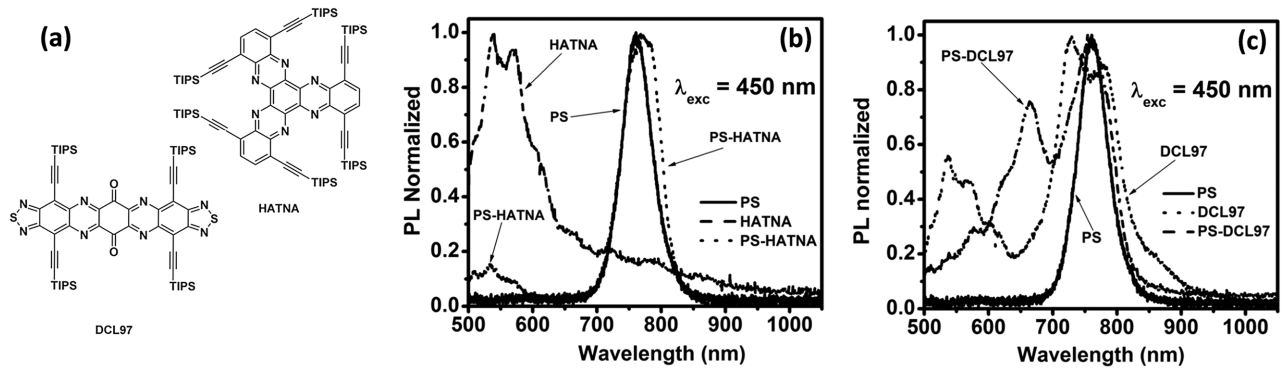


**Figure 1.** a) Scheme of the additives studied in this work. Normalized photoluminescence of perovskite (PS) reference layer. b) HATNA film and PS with HATNA film and c) DCL97 and PS with DCL97.

by a factor of 2–4 and the reduction of the light amplification threshold energy by a factor of 2–4 when organic additives are used. A systematic characterization of $CH_3NH_3PbI_3$ with additives points to a reduction in the non-radiative carrier recombination paths by the passivation of PS interface and grain boundaries in the polycrystalline film. The main scope of this work is to present a general method in order to increase the efficiency of perovskite-based optoelectronic devices (solar cells, LEDs, and optical amplifiers), without introducing any additional step, and even using different anti-solvent. The method proposed in the present paper offers the possibility to deposit perovskite mixed with many different organic and inorganic compounds, and opens a broad range of applications on perovskite optoelectronic devices as solar cells, LEDs, and lasers.

There are several examples of the use of additives for the improvement of perovskite solar cells (PSCs). In most of the cases, these additives are introduced by dissolving them in the solution containing the perovskite precursors,[21] and in other cases a gaseous post treatment after the perovskite-film formation is used.[14] When additives are incorporated to the solution of perovskite precursors, they play an important role in the growth of perovskite film and have an important impact in the film morphology. However, this method is restricted only to additives soluble in the non-polar solution with perovskite precursors.[21] Pyridine vapor exposure of a perovskite film decreases significantly the non-radiative recombination, however this method introduces an additional preparation step.[14] For other perovskite optoelectronic devices, there are significantly lower number of reports on the use of additives. Cho et al. reported record LED efficiencies by the use of 2,2′,2″-(1,3,5-benzinetriyl)-tris(1-phenyl-1-H-benzimidazole) (TPBI) additive dissolved in chloroform and using a multistep nanocrystal pinning process.[8b] This deposition process produces nanocrystalline grains, increasing the LED current efficiency. However, this small grain size morphology does not seem to be optimum for solar cells.

We have developed a new approach that takes advantage of the anti-solvent deposition method,[11b,c,18] that is, the method with which the highest PSC record efficiencies have been reported.[11a,22] In this method, during the spin-coating of *N,N*-dimethylformamide (DMF) solution, containing $CH_3NH_3PbI_3$ (hereafter $MAPbI_3$) precursors (methylammonium iodide (MAI) and $PbI_2$), the sample is exposed to a second solvent with a non-polar character in which perovskite precursors are not soluble. This exposure produces the saturation of the solution and the fast precipitation of the precursors creating numerous perovskite nucleation centers and the corresponding formation of a flat, uniform, and pinhole-free perovskite layer. Our approach consists of dissolving the additives in the anti-solvent and introduce them in the layer during the anti-solvent step, see the Experimental Section for more details.

HATNA and DCL97 are not soluble in DMF, which is the common solvent used for PS film fabrication. In this way, to combine PS and the organic compound in a single film, we dispersed the organic additive in an anti-solvent, which was used in the film preparation. Thin films of PS, organic additives, and PS with the organic additive using the anti-solvent method have been deposited on glass substrates. The PL spectra of these layers are plotted in Figure 1b,c, for samples containing HATNA and DCL97, respectively. The PL spectra of PS and organic single layers are in good agreement with previous reports.[12a,19a,20] The PL of perovskite layer containing additives, hereafter PS-HATNA and PS-DCL97, presents PL traces of both compounds, as observed in Figure 1b,c, respectively, indicating their presence in the final film after the anti-solvent process. Note that in the case of PS-DCL97, Figure 1c, a new feature at ≈650 nm not present in any of the PL spectra of the single layers is observed for the mixed sample. This peak is probably originated in the interaction between both materials, being its interpretation beyond the scope of this paper and it is under current research.

We have not limited our study to a single type of devices and have extended the study to three different optoelectronic devices: solar cells, LEDs, and waveguide optical amplifiers to demonstrate the versatility of this general approach for the optoelectronic field. Solar cells were prepared using compact $TiO_2$ and (2,2′,7,7′-tetrakis(*N,N*-di-*p*-methoxyphenylamine)-9,9-spirobifluorene) (spiro-OMeTAD) as electron and hole selective contacts, respectively. Two configurations, planar and with $TiO_2$ mesoporous scaffold, have been analyzed. The current–voltage (*J–V*) curve for the prepared solar cells showed that the presence of the organic compounds improved the device performance depending on the organic concentration, see Figure S1 and Table S1 (Supporting Information). The concentration dependence study has been carried out preparing planar PSC samples with the following configuration: glass/FTO/compact $TiO_2$/PS or PS-HATNA or PS-DCL97/spiro-OMeTAD/Au, using

chlorobenzene as anti-solvent. An increase of device efficiency, mainly due to an increase of the photocurrent, has been detected depending on the concentration, observing the highest increase for 50 and 37.5 mg $mL^{-1}$ for HATNA and DCL97 (see Table S1, Supporting Information), respectively. In addition, solar cells containing mesoporous $TiO_2$ layer have been prepared with the following configuration: glass/FTO/compact $TiO_2$/mesoporous $TiO_2$/PS or PS-HATNA or PS-DCL97/spiro-OMeTAD/Au. For mesoporous configuration HATNA, 50 mg $mL^{-1}$, was introduced using diethyl ether as the anti-solvent. HATNA presents good solubility on both diethyl ether and chlorobenzene, but high-efficiency reference cells are obtained with diethyl ether instead of chlorobenzene. DCL97 is not soluble in diethyl ether and consequently chlorobenzene has been chosen as anti-solvent in that case, allowing us to show the versatility of the method as it can be employed with different solvents. For $TiO_2$ mesoporous PSCs, all the photovoltaic parameters (short-circuit current, $J_{sc}$, open-circuit voltage, $V_{oc}$, fill factor, FF, and photoconversion efficiency, $\eta$) increase for the PS-HATNA sample in comparison with the reference PS sample, see **Figure 2**a and Table S2 (Supporting Information). Concretely, efficiency moves from close to 12% for the reference sample to close to 15% for PS-HATNA, see Table S2 (Supporting Information), increasing a significant ≈25%. It is also important to highlight that the PS-HATNA device is practically hysteresis free, see Figure 2a. In addition, PS-HATNA also presents a better long-term stability behavior, see Figure S2 and Table S2 (Supporting Information). The analysis of incident-photon-to-current efficiency (IPCE) shows a good agreement between the integrated photocurrent, see Figure 2b, and the $J_{sc}$ measured in the $J$–$V$ curve, see Figure 2a. In addition, IPCE unveils that the enhancement in the photocurrent for PS-HATNA samples is not due to the light harvesting (and subsequent charge collection) from HATNA molecules. IPCE for PS-HATNA has the same spectra that for the PS reference sample with an increased efficiency in all the wavelength range, and especially at longer wavelengths where light absorption of HATNA compound is negligible,[19a] see Figure 2b. These results indicate a clear enhancement of the perovskite layer performance by the use of HATNA additive rather than an improvement of the co-absorption by the presence of HATNA. In the case of DCL97, samples with configuration glass/FTO/compact $TiO_2$/mesoporous$TiO_2$/PS or PS-DCL97/spiro-OMeTAD/Au were also prepared, using chlorobenzene as the anti-solvent. In that case the efficiency of PS-DCL97 has increased ≈75% with respect to a reference cell prepared with chlorobenzene anti-solvent. However in this case, the reference samples without DCL97 are far away from optimization presenting a low efficiency, 5%, see Table S3 (Supporting Information) for more details. Independently of the configuration, employed molecule, and anti-solvent, we have observed systematically an increase of efficiency of the prepared solar cells with respect to the reference samples when additives were used, highlighting the huge potentiality of the method to improve the device performance. Higher efficiencies can be expected after an accurate optimization process at each concrete configuration.

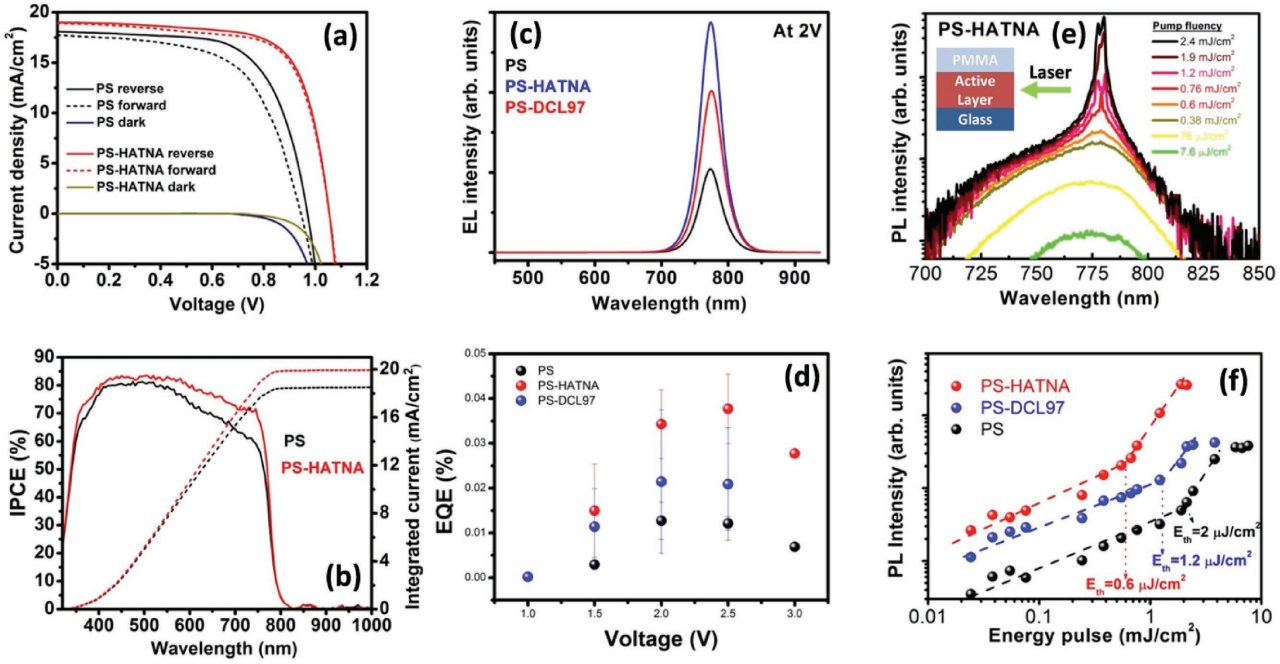


**Figure 2.** a) Current–potential curve of a perovskite reference solar cell and of a perovskite with HATNA additive introduced during the anti-solvent step, under dark and under 1 sun illumination, forward and reverse scans are plotted in order to show the hysteresis behavior. b) Incident-photon-to-current efficiency (right axis, solid lines) and the integrated photocurrent (left axis, dashed lines) of the devices depicted in (a). c) Electroluminescence of LEDs prepared with perovskite and perovskite with HATNA and DCL97 additives as active layer at an applied forward bias of 2 V. d) External quantum efficiency on the prepared LEDs. e) Photoluminescence obtained with side excitation,[9] see inset, of perovskite with HATNA additive deposited on glass and with a PMMA capping, see inset. Sample PL has been recorded with different excitation powers. f) PL intensity as function of excitation power of perovskite reference and perovskite with HATNA and DCL97 additives films sandwiched between glass and PMMA layers.

$MAPbI_3$ perovskite thin film with organic additives prepared by our method can be applied not only for increasing the performance of light harvesting devices but also for light-emitting systems. LEDs were prepared using PS, PS-HATNA, and PS-DCL97 as active layers, and compact $TiO_2$ and spiro-OMeTAD as electron and hole transport materials, respectively, following a previously reported configuration.[8a] The electroluminescence (EL) spectra of all the samples (PS, PS-HATNA, and PS-DCL97) show only a peak corresponding to the perovskite emission with no parasitic contributions from the organic additives, see Figure 2c. The fabricated LEDs present a remarkably low threshold energy, as low as the $MAPbI_3$ bandgap, see Figure 2d. The use of additives has increased the EQE by a factor of 2 and 4 for DCL97 and HATNA, respectively, as observed in Figure 2d. The EQE presents its maximum value with an applied bias of 2 V for the PS and PS-DCL97 samples, while for the PS-HATNA devices the maximum is observed at 2.5 V.

We have also investigated the anti-solvent deposition of additives in perovskite films for light amplification. Waveguide optical amplifier devices were prepared using PS reference layer or PS with organic additives (HATNA or DCL97) as active layer sandwiched between glass and PMMA layer, see inset Figure 2e, following a configuration previously developed by us.[9] These active layers were excited by one of their side faces, see inset Figure 2e, by means of a pulsed laser at 533 nm. Figure 2e shows the emitted light spectra measured at the opposite face end for the PS-HATNA sample at different pump powers. The spectra for PS and PS-DCL97 planar waveguides are plotted in Figure S3 (Supporting Information). Waveguided PL spectra correspond to that of the perovskite layer centered around 780 nm, but collapse into a narrow line for high enough pump fluencies (see Figure 2e), which integrated intensity grows superlinearly, as observed in Figure 2f. Both are clear signatures of stimulated emission that exhibits a reduction of the energy threshold by factor of 2 or 4, when the additives DCL97 or HATNA are incorporated, respectively, into the PS film (Figure 2f and Figure S3, Supporting Information). Another characteristic signature of the stimulated-emission regime is the decrease of the PL recombination time. Time-resolved PL (TRPL) analysis has been carried out to determine the characteristic decay time of the waveguided PL (Figure S4, Supporting Information) that reached our experimental system temporal response (and consequently cannot be further determined) for pump fluencies higher than 0.72, 0.5, and 0.1 nJ for PS, PS-DCL97, and PS-HATNA samples, respectively, in good agreement with the lower stimulated-emission energy threshold observed in Figure 2f for films made by incorporating additives.

To gain further insight into the origin of the general enhancement in device performance observed for perovskite optoelectronic devices (i.e., solar cells, LEDs, and optical amplifiers), a systematic characterization by X-ray diffraction (XRD), scanning electron microscopy (SEM), and impedance spectroscopy (IS) has been carried out. XRD spectra of the films of perovskite with additive do not present any significant variation with respect to reference perovskite layer produced without additives, see Figure S6 (Supporting Information), indicating no change in the crystallite size or in the preferential orientation. Moreover, a systematic characterization of the perovskite films prepared with and without additives has been carried out, see Figure S7 (Supporting Information). The use of additives has a clear interfacial effect. While the use of HATNA produces an organic capping layer, that is removed when spiro-OMeTAD is deposited, the addition of DCL97 changes the roughness and surface morphology, but with no change of perovskite grain size in both cases, see Section S7 and Figure S7 (Supporting Information) for more details. Consequently, a first effect of the additives is the modification of the interface that could induce a beneficial effect in the final cell performance.

PS and PS-HATNA with mesoporous $TiO_2$ configuration have been analyzed under 0.09 sun intensity at different applied voltages. The obtained Nyquist plots at 0 V are plotted in **Figure 3**a. Two basic features at high and lower frequencies are observed. The impedance spectra have been fitted using the equivalent circuit recently reported, see Figure S5 (Supporting Information). Figure 3b plots the resistance of the low-frequency arc, $R_1$, obtained from the fitting of impedance spectra. $R_1$ is related to the charge carrier recombination (i.e., inversely related with the recombination rate).[23] Figure 3b shows the increase in recombination resistance when HATNA additive was introduced into PS film, indicating that the efficiency enhancement observed for devices with additives are due to a decrease of recombination. Dark *J–V* curves, see Figure 2a, and open-circuit voltage decay, see Figure S8 (Supporting Information), are also in agreement with this conclusion. Impedance spectroscopy cannot determine the origin of the recombination mechanism. However, radiative recombination in perovskite solar cells has been characterized by time-resolved PL, from which we deduce PL decay times in the order of tens-hundreds of ns,[4,12b] consequently the recombination paths detected by impedance at the µs range and slower scales have a different origin, probably related to non-radiative centers.

Finally, to understand in which way the additives introduced by the anti-solvent deposition method reduces recombination in the perovskite layers beyond the interfacial effect, a PL mapping of the film surface has been carried out using a commercial Scientific Xplora micro-Raman system with 533 and 638 nm laser excitation. The integration of PL at different detection wavelengths, $\lambda_{det}$, for PS-DCL97 sample and the subtraction of the PS PL allows to obtain a mapping of the DCL97 PL, Figure 3d, and PS PL, Figure 3e, see Figure S9 (Supporting Information) for further details of the decoupling of both PL contributions. These results have been doubly checked by using a second excitation wavelength, $\lambda_{exc}$ = 638 nm, see Figure 3f. Comparing, the PL maps in Figure 3d,e are clearly complementary: the maximum intensities of PL from DCL97 are observed in areas where the PL from PS is minimum and vice versa. Moreover, the observed PL valleys and peaks form a network with features of hundreds nm size, similar to the grain size observed in PS films by SEM (Figure 3c). A similar analysis performed on different parts of the PS-DCL97 sample surface yielded analogous results, as shown in Figure S10 (Supporting Information) for the PL map in a different place of the sample surface. This complementary PL emission coinciding with the perovskite grain size indicates the hypothesis that DCL97 molecules tend to locate at the grain boundaries of the perovskite film. Hence, the introduction of additives decreases the recombination by the passivation of the grain boundaries. Passivation of grain boundaries has previously shown beneficial effects for

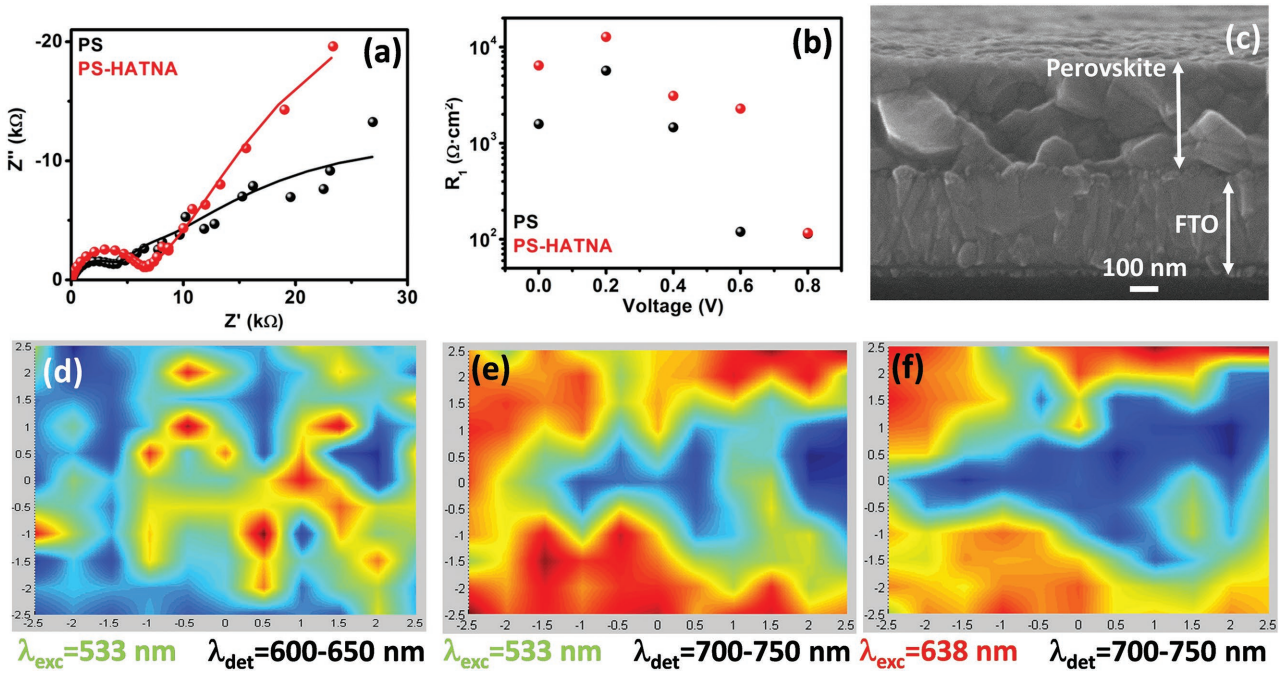


**Figure 3.** a) Nyquist plot of perovskite and perovskite with HATNA additive solar cells, plotted in Figure 2a, with mesoporous $TiO_2$ configuration and using diethyl ether as anti-solvent, under 0.09 sun illumination at 0 V applied bias. Symbols correspond to the experimental points while solid line is the fitting of the impedance spectra using equivalent circuit in Figure S5 (Supporting Information).[24] b) $R_1$ resistance related with the recombination resistance of perovskite and perovskite with HATNA additive solar cells.[23] c) SEM picture of a cross section of perovskite planar layer film. Photoluminescence intensity map of a sample of perovskite with DCL97 additive, excitation wavelength, $\lambda_{exc}$, and the range of detected wavelengths, $\lambda_{det}$, are indicated in each map. d) PL from DCL97, where PL from perovskite has been subtracted, see Figure S9 (Supporting Information), for further details. e,f) PL from perovskite, see Figure S9 (Supporting Information) for further details, for two different $\lambda_{exc}$. Vertical and horizontal scales for the maps are in µm.

the increase of the solar-cell photoconversion efficiency,[15] PL emission,[14] and the stability of PS devices.[25]

Through this versatile and general approach (three different optoelectronic devices, two different additive molecules, two different configurations with mesoporous scaffold and planar devices, two different solvents used in the anti-solvent step) we observe a systematic increase of performance in all the devices when additives are used. In this work, we show by XRD that additives do not produce a change in the crystallite size or preferential orientation, while grain size is not modified as it has been determined by the SEM analysis. The main role of additives is the passivation of the grain boundaries and/or perovskite interface for electron-deficient N-PAHs produces a reduction of non-radiative recombination that leads to a notable increase of the main figures of merit of perovskite optoelectronic devices, including solar cells, LEDs, and optical amplifiers. The process consists in the introduction of additives in an anti-solvent during the perovskite spin-coating deposition. We have used this method to increase systematically the performance of perovskite solar cells with planar and mesoscopic configurations, the EQE of perovskite LEDs by a factor of 2–4, and to reduce the stimulate emission threshold by a factor of 2–4 by the introduction of DCL97 and HATNA additives in comparison with devices prepared in the same way with the same anti-solvent but without additives. The use of DCL97 and HATNA additives has allowed us to verify the presence of the additives in the prepared film by PL measurements and to track the final situation of these molecules in the film, detecting their presence at the grain boundaries. We have also observed a decrease of the PS recombination due to the use of additives by impedance spectroscopy. These observations point to a passivating effect of the grain boundaries and/or interface by the introduction of additives. It is important to highlight that it is a general method that can be used for the introduction of a broad range of different additives. The design of specific additives with particular properties or functionalizations can enhance further the performance of the optoelectronic devices. For example, the lower threshold energy obtained for the PS-HATNA films in comparison to the PS-DCL97 is probably due to the fact that HATNA does not absorb light at the excitation wavelength, but still passivating the perovskite layer. This work opens an interesting research field on the interaction of perovskite with other compounds with important implications in the enhancement of the perovskite optoelectronic devices.

## Experimental Section

*Synthesis of HATNA and DCL97*: The synthesis of HATNA[16i,19] and DCL97[20] was carried out following previously reported methods and scaled-up accordingly to obtain ≈100 mg batches.

*$TiO_2$ Compact Layer*: $SnO_2$:F (FTO) substrates were cleaned with soap, sonicated in distilled water, ethanol, and a mixture of acetone/isopropanol (30:70 v/v ratio) for 15 min and then treated with an UV (ultraviolet)–$O_3$ lamp for 15 min. The $TiO_2$ compact layers were manually deposited by spray pyrolysis at 450 °C, consuming 5 mL of

a solution of titanium di-isopropoxide bis(acetylacetonate, 75% vol. 2-propanol) in absolute ethanol (1:9, v/v ratio); the films were annealed at 450 °C for 30 min.

*$TiO_2$ Mesoporous (Scaffold)*: $TiO_2$ paste (Dyesol 30NRd, 30 nm average particle size) dissolved in absolute ethanol (150 mg $mL^{-1}$) was spin-coated on $TiO_2$ compact layers at 1500 rpm. The films were pre-heated at 100 °C for 10 min and then at 500 °C for 30 min.

*Perovskite Solution*: 622 mg (1.35 mmol) of $PbI_2$ was added in the solution containing 1 mL of DMF and 95 µL of dimethyl sulfoxide (DMSO). This solution was heated at 65 °C to dissolve $PbI_2$ and then cooled to room temperature. Subsequently, $PbI_2$ solution was poured into a container containing 215 mg (1.35 mmol) of MAI to make final solution for PS deposition.

*Perovskite-Film Deposition*: PS films were prepared by spin-coating at 4000 rpm for substrates with mesoporous $TiO_2$ scaffolds and at 5000 rpm for substrates only with $TiO_2$ compact layer. Anti-solvent (chlorobenzene or diethyl ether), ≈200 µL, was poured in the films when the spin coater was running after 7 s of the spinning start. Perovskite films were annealed at 65 °C for 1 min and consequently 100 °C for 2 min.

*Organic Additive Solutions*: HATNA and DCL97 solutions were prepared by dissolving HATNA or DCL97 in anti-solvent (diethyl ether and chlorobenzene, respectively) separately with the concentration varying from 12.5 to 50 mg $mL^{-1}$. Reference perovskite films have been prepared using both solvents, diethyl ether and chlorobenzene, during the anti-solvent step but without additives. For a fair comparison each sample prepared with additives is compared with a reference perovskite sample which was prepared using the same solvent during the anti-solvent step.

*Spiro-OMeTAD and Gold*: Spiro-OMeTAD solution was prepared by dissolving 72.3 mg spiro-OMeTAD in 1 mL of chlorobenzene, and then mixed with 28.8 µL of 4-*tert*-butylpyridine and 17.5 µL of a stock $Li^+$ solution (which contained 520 mg $mL^{-1}$ bis-trifluoromethylsulfonylamine lithium salt in acetonitrile). Spiro-OMeTAD layer was spin-coated on PS or PS with additives films at 4000 rpm for 30 s. Finally, 60 nm of gold were thermally evaporated in an ultrahigh vacuum chamber on top of a spiro-OMeTAD layer as charge extracting contact.

*Characterization*: The morphology of the films was analyzed by SEM using a JSM7001F (field emission scanning electron microscope). *J–V* curves of solar cells were measured under a xenon arc lamp simulator equipped with an AM 1.5 spectral filter (Sun 2000, ABET Technologies). The intensity was adjusted to provide 1 sun (100 mW $cm^{-2}$) by using a calibrated silicon solar cell. The *J–V* characteristics were recorded by scanning the potential from high voltage to zero (reverse mode) and from zero to high voltage (forward mod) at ≈45 mV $s^{-1}$. The IPCE measurements were performed employing a 150 W xenon lamp coupled with a computer-controlled monochromator; the photocurrent was measured using an optical power meter 70310 from Oriel Instruments, using a Si photodiode to calibrate the system. The impedance spectroscopy measurements were performed under 0.09 sun illumination, calibrated with an NREL-calibrated Si solar cell, and under $N_2$ flow. The measurements were carried out by means of a FRA equipped PGSTAT-30 from Autolab at different forward voltage bias and applying a 20 mV voltage AC perturbation over the constant applied bias with the frequency ranging between 1 MHz and 0.05 Hz. The use of 0.09 sun illumination prevents cell degradation during the impedance measurement, see Figure S11 (Supporting Information), and also keep the illumination conditions as it has been shown that working conditions of perovskite layer vary significantly when the layer is illuminated.[24b] The EL spectra of LED devices based on PS absorber without and with organic compounds (HATNA or DCL97) in situ were obtained by using a spectrophotometer based on a CCD detector (Andor-iDUSDV420A-OE) synchronized with the potentiostat (Gamry Reference 3000). The combination of both apparatus allowed registering optical variations (absorbance, transmittance, light emission, etc.) while applying an external electrical stimulus (voltage or current) with a maximum time resolution on the milliseconds scale. EL measurements have been carried out under dark conditions and under $N_2$ flow at room temperature. The EQE measurements were performed by calibrating the optical equipment with a commercial GaAs infrared LED (model EL-23G, peak emission centered at $\lambda_{max}$ = 940 nm, 28.3 W $sr^{-1}$ $m^{-2}$). PL experiments were carried out by pumping the surface of the samples with a 533 nm DSPP (diode pumped solid state) laser and a 780 nm semiconductor diode. Back-scattered PL was then collected with the aid of a microscope objective and dispersed in an Ocean Optics HR4800 spectrograph.

Stimulated-emission experiments were performed by exciting the surface of the samples with an Nd:YAG 533 nm pulsed laser (1 ns, 20 kHz) and collecting the emitted PL with a 20× microscope objective. PL spectra were obtained by dispersing the light in an Ocean Optics HR4800 spectrograph, and TRPL were carried out by focusing the PL into a Hamamatsu C5658-3769 avalanche photodetector connected to a BOXCARDPCS-150 electronics from Becker & Hickl GmbH. The PL maps were obtained by using a commercial Scientific Xplora micro-Raman system with 533 and 638 nm laser excitation. XRD has been characterized employing a Bruker AXS-D4 Endeaver Advance X-ray diffractometer using Cu $K_\alpha$ radiation.

## Supporting Information

Supporting Information is available from the Wiley Online Library or from the author.

## Acknowledgements

The work was supported by MINECO of Spain (Project Nos. MAT2013-47192-C3-1-R, MAT2015-70611-ERC, and TEC2014-53727-C2-1-R) and by Generalitat Valenciana (Project Nos. PROMETEOII/2014/020 and PROMETEOII/2014/059). The authors acknowledge SCIC from University Jaume I for help with SEM and XRD characterization. A.M.-A. is grateful to the Basque Foundation for Science (Ikerbasque), POLYMAT, the University of the Basque Country (SGIker), the Deutsche Forschungsgemeinschaft (AU 373/3-1 and MA 5215/4-1), Gobierno de España (MINECO MAT2012-35826, CTQ2015-71936-REDT and CTQ2016-77970-R), Gobierno Vasco (BERC program and PC2015-1-01(06-37)), Diputación Foral de Guipúzcoa (2015-CIEN-000054-01 and OF215/2016(ES)), and the European Union (ERA-Chemistry, Career Integration Grant No. 618247 and FEDER).

Received: July 30, 2016
Revised: October 14, 2016
Published online: December 15, 2016

[1] a) T. M. Brenner, D. A. Egger, L. Kronik, G. Hodes, D. Cahen, *Nat. Rev. Mater.* **2016**, *1*, 15007; b) M. A. Green, A. Ho-Baillie, H. J. Snaith, *Nat. Photonics* **2014**, *8*, 506; c) S. D. Stranks, H. J. Snaith, *Nat. Nanotechnol.* **2015**, *10*, 391; d) B. R. Sutherland, E. H. Sargent, *Nat. Photonics* **2016**, *10*, 295.

[2] S. De Wolf, J. Holovsky, S.-J. Moon, P. Löper, B. Niesen, M. Ledinsky, F.-J. Haug, J.-H. Yum, C. Ballif, *J. Phys. Chem. Lett.* **2014**, *5*, 1035.

[3] a) W.-J. Yin, T. Shi, Y. Yan, *Adv. Mater.* **2014**, *26*, 4653; b) W.-J. Yin, T. Shi, Y. Yan, *Appl. Phys. Lett.* **2014**, *104*, 063903.

[4] a) S. D. Stranks, G. E. Eperon, G. Grancini, C. Menelaou, M. J. P. Alcocer, T. Leijtens, L. M. Herz, A. Petrozza, H. J. Snaith, *Science* **2013**, *342*, 341; b) G. Xing, N. Mathews, S. Sun, S. S. Lim, Y. M. Lam, M. Grätzel, S. Mhaisalkar, T. C. Sum, *Science* **2013**, *342*, 344.

[5] a) W. Tress, N. Marinova, O. Inganäs, M. K. Nazeeruddin, S. M. Zakeeruddin, M. Graetzel, *Adv. Energy Mater.* **2015**, *5*, 1400812; b) J. S. Manser, P. V. Kamat, *Nat. Photonics* **2014**, *8*, 737; c) D. Bi, W. Tress, M. I. Dar, P. Gao, J. Luo, C. Renevier, K. Schenk, A. Abate, F. Giordano, J.-P. Correa Baena, J.-D. Decoppet,

S. M. Zakeeruddin, M. K. Nazeeruddin, M. Grätzel, A. Hagfeldt, *Sci. Adv.* **2016**, *2*, e1501170.
[6] M. A. Green, K. Emery, Y. Hishikawa, W. Warta, E. D. Dunlop, *Prog. Photovoltaics* **2016**, *24*, 905.
[7] A. Kojima, K. Teshima, Y. Shirai, T. Miyasaka, *J. Am. Chem. Soc.* **2009**, *131*, 6050.
[8] a) O. A. Jaramillo-Quintero, R. S. Sanchez, M. Rincon, I. Mora-Sero, *J. Phys. Chem. Lett.* **2015**, *6*, 1883; b) H. Cho, S.-H. Jeong, M.-H. Park, Y.-H. Kim, C. Wolf, C.-L. Lee, J. H. Heo, A. Sadhanala, N. Myoung, S. Yoo, S. H. Im, R. H. Friend, T.-W. Lee, *Science* **2015**, *350*, 1222; c) Z.-K. Tan, R. S. Moghaddam, M. L. Lai, P. Docampo, R. Higler, F. Deschler, M. Price, A. Sadhanala, L. M. Pazos, D. Credgington, F. Hanusch, T. Bein, H. J. Snaith, R. H. Friend, *Nat. Nanotechnol.* **2014**, *9*, 687; d) L. Gil-Escrig, G. Longo, A. Pertegas, C. Roldan-Carmona, A. Soriano, M. Sessolo, H. J. Bolink, *Chem. Commun.* **2015**, *51*, 569; e) Y.-H. Kim, H. Cho, J. H. Heo, T.-S. Kim, N. Myoung, C.-L. Lee, S. H. Im, T.-W. Lee, *Adv. Mater.* **2015**, *27*, 1248.
[9] I. Suárez, E. J. Juárez-Pérez, J. Bisquert, I. Mora-Seró, J. P. Martínez-Pastor, *Adv. Mater.* **2015**, *27*, 6157.
[10] a) G. Xing, N. Mathews, S. S. Lim, N. Yantara, X. Liu, D. Sabba, M. Grätzel, S. Mhaisalkar, T. C. Sum, *Nat. Mater.* **2014**, *13*, 476; b) F. Deschler, M. Price, S. Pathak, L. E. Klintberg, D.-D. Jarausch, R. Higler, S. Hüttner, T. Leijtens, S. D. Stranks, H. J. Snaith, M. Atatüre, R. T. Phillips, R. H. Friend, *J. Phys. Chem. Lett.* **2014**, *5*, 1421; c) H. Zhu, Y. Fu, F. Meng, X. Wu, Z. Gong, Q. Ding, M. V. Gustafsson, M. T. Trinh, S. Jin, X. Y. Zhu, *Nat. Mater.* **2015**, *14*, 636.
[11] a) W. S. Yang, J. H. Noh, N. J. Jeon, Y. C. Kim, S. Ryu, J. Seo, S. I. Seok, *Science* **2015**, *348*, 1234; b) N. J. Jeon, J. H. Noh, Y. C. Kim, W. S. Yang, S. Ryu, S. I. Seok, *Nat. Mater.* **2014**, *13*, 897; c) N. Ahn, D.-Y. Son, I.-H. Jang, S. M. Kang, M. Choi, N.-G. Park, *J. Am. Chem. Soc.* **2015**, *137*, 8696.
[12] a) T. T. Ngo, I. Suarez, R. S. Sanchez, J. P. Martinez-Pastor, I. Mora-Sero, *Nanoscale* **2016**, *8*, 14379; b) R. S. Sanchez, M. S. de la Fuente, I. Suarez, G. Muñoz-Matutano, J. P. Martinez-Pastor, I. Mora-Sero, *Sci. Adv.* **2016**, *2*, e1501104; c) X. Gong, Z. Yang, G. Walters, R. Comin, Z. Ning, E. Beauregard, V. Adinolfi, O. Voznyy, E. H. Sargent, *Nat. Photonics* **2016**, *10*, 253; d) Z. Ning, X. Gong, R. Comin, G. Walters, F. Fan, O. Voznyy, E. Yassitepe, A. Buin, S. Hoogland, E. H. Sargent, *Nature* **2015**, *523*, 324; e) S.-S. Li, C.-H. Chang, Y.-C. Wang, C.-W. Lin, D.-Y. Wang, J.-C. Lin, C.-C. Chen, H.-S. Sheu, H.-C. Chia, W.-R. Wu, U. S. Jeng, C.-T. Liang, R. Sankar, F.-C. Chou, C.-W. Chen, *Energy Environ. Sci.* **2016**, *9*, 1282.
[13] S. F. Völker, S. Collavini, J. L. Delgado, *ChemSusChem* **2015**, *8*, 3012.
[14] D. W. de Quilettes, S. M. Vorpahl, S. D. Stranks, H. Nagaoka, G. E. Eperon, M. E. Ziffer, H. J. Snaith, D. S. Ginger, *Science* **2015**, *348*, 683.
[15] Y. Shao, Z. Xiao, C. Bi, Y. Yuan, J. Huang, *Nat. Commun.* **2014**, *5*, 5784.
[16] a) A. Mateo-Alonso, *Chem. Soc. Rev.* **2014**, *43*, 6311; b) U. H. F. Bunz, J. U. Engelhart, B. D. Lindner, M. Schaffroth, *Angew. Chem., Int. Ed.* **2013**, *52*, 3810; c) U. H. F. Bunz, *Chem.–Eur. J.* **2009**, *15*, 6780; d) M. Stępień, E. Gońka, M. Żyła, N. Sprutta, *Chem. Rev.* **2016**, DOI: 10.1021/acs.chemrev.6b00076; e) A. B. Marco, C. Gozalvez, M. Olano, X. Sun, A. Atxabal, M. Melle-Franco, L. E. Hueso, A. Mateo-Alonso, *Phys. Chem. Chem. Phys.* **2016**, *18*, 11616; f) L. Jiang, A. C. Papageorgiou, S. C. Oh, Ö. Sağlam, J. Reichert, D. A. Duncan, Y.-Q. Zhang, F. Klappenberger, Y. Guo, F. Allegretti, S. More, R. Bhosale, A. Mateo-Alonso, J. V. Barth, *ACS Nano* **2016**, *10*, 1033; g) A. B. Marco, D. Cortizo-Lacalle, C. Gozalvez, M. Olano, A. Atxabal, X. Sun, M. Melle-Franco, L. E. Hueso, A. Mateo-Alonso, *Chem. Commun.* **2015**, *51*, 10754; h) R. Garcia, M. Melle-Franco, A. Mateo-Alonso, *Chem. Commun.* **2015**, *51*, 8037; i) D. Cortizo-Lacalle, A. Pertegas, L. Martinez-Sarti, M. Melle-Franco, H. J. Bolink, A. Mateo-Alonso, *J. Mater. Chem. C* **2015**, *3*, 9170; j) S. More, S. Choudhary, A. Higelin, I. Krossing, M. Melle-Franco, A. Mateo-Alonso, *Chem. Commun.* **2014**, *50*, 1976; k) S. More, R. Bhosale, A. Mateo-Alonso, *Chem.–Eur. J.* **2014**, *20*, 10626; l) M. Grzelczak, N. Kulisic, M. Prato, A. Mateo-Alonso, *Part. Part. Syst. Charact.* **2014**, *31*, 121; m) R. García, S. More, M. Melle-Franco, A. Mateo-Alonso, *Org. Lett.* **2014**, *16*, 6096; n) S. More, R. Bhosale, S. Choudhary, A. Mateo-Alonso, *Org. Lett.* **2012**, *14*, 4170; o) N. Kulisic, S. More, A. Mateo-Alonso, *Chem. Commun.* **2011**, *47*, 514; p) A. Mateo-Alonso, N. Kulisic, G. Valenti, M. Marcaccio, F. Paolucci, M. Prato, *Chem. Asian J.* **2010**, *5*, 482; q) M. Grzelczak, N. Kulisic, M. Prato, A. Mateo-Alonso, *Chem. Commun.* **2010**, *46*, 9122; r) A. Mateo-Alonso, C. Ehli, K. H. Chen, D. M. Guldi, M. Prato, *J. Phys. Chem. A* **2007**, *111*, 12669; s) A. M. Alonso, R. Horcajada, M. Motevalli, J. H. P. Utley, P. B. Wyatt, *Org. Biomol. Chem.* **2005**, *3*, 2842; t) A. M. Alonso, R. Horcajada, H. J. Groombridge, R. Chudasama, M. Motevalli, J. H. P. Utley, P. B. Wyatt, *Org. Biomol. Chem.* **2005**, *3*, 2832; u) A. M. Alonso, R. Horcajada, H. J. Groombridge, R. Mandalia, M. Motevalli, J. H. P. Utley, P. B. Wyatt, *Chem. Commun.* **2004**, 412; v) G. J. Richards, J. P. Hill, T. Mori, K. Ariga, *Org. Biomol. Chem.* **2011**, *9*, 5005; w) U. H. F. Bunz, *Pure Appl. Chem.* **2010**, *82*, 953; x) G. J. Richards, J. P. Hill, N. K. Subbaiyan, F. D'Souza, P. A. Karr, M. R. J. Elsegood, S. J. Teat, T. Mori, K. Ariga, *J. Org. Chem.* **2009**, *74*, 8914.
[17] a) J. E. Anthony, A. Facchetti, M. Heeney, S. R. Marder, X. Zhan, *Adv. Mater.* **2010**, *22*, 3876; b) Z. Liang, Q. Tang, J. Liu, J. Li, F. Yan, Q. Miao, *Chem. Mater.* **2010**, *22*, 6438.
[18] M. Xiao, F. Huang, W. Huang, Y. Dkhissi, Y. Zhu, J. Etheridge, A. Gray-Weale, U. Bach, Y.-B. Cheng, L. Spiccia, *Angew. Chem.* **2014**, *126*, 10056.
[19] a) G. Tregnago, C. Fléchon, S. Choudhary, C. Gozalvez, A. Mateo-Alonso, F. Cacialli, *Appl. Phys. Lett.* **2014**, *105*, 143304; b) F. Selzer, C. Falkenberg, M. Hamburger, M. Baumgarten, K. Müllen, K. Leo, M. Riede, *J. Appl. Phys.* **2014**, *115*, 054515; c) J. Clark, R. Archer, T. Redding, C. Foden, J. Tant, Y. Geerts, R. H. Friend, C. Silva, *J. Appl. Phys.* **2008**, *103*, 124510.
[20] D. Cortizo-Lacalle, C. Gozalvez, M. Olano, X. Sun, M. Melle-Franco, L. E. Hueso, A. Mateo-Alonso, *Org. Lett.* **2015**, *17*, 5902.
[21] a) X. Li, M. Ibrahim Dar, C. Yi, J. Luo, M. Tschumi, S. M. Zakeeruddin, M. K. Nazeeruddin, H. Han, M. Grätzel, *Nat. Chem.* **2015**, *7*, 703; b) P.-W. Liang, C.-Y. Liao, C.-C. Chueh, F. Zuo, S. T. Williams, X.-K. Xin, J. Lin, A. K. Y. Jen, *Adv. Mater.* **2014**, *26*, 3748; c) C.-Y. Chang, C.-Y. Chu, Y.-C. Huang, C.-W. Huang, S.-Y. Chang, C.-A. Chen, C.-Y. Chao, W.-F. Su, *ACS Appl. Mater. Interfaces* **2015**, *7*, 4955; d) Q. Dong, Z. Wang, K. Zhang, H. Yu, P. Huang, X. Liu, Y. Zhou, N. Chen, B. Song, *Nanoscale* **2016**, *8*, 5552; e) C.-C. Chueh, C.-Y. Liao, F. Zuo, S. T. Williams, P.-W. Liang, A. K. Y. Jen, *J. Mater. Chem. A* **2015**, *3*, 9058.
[22] M. Saliba, T. Matsui, J.-Y. Seo, K. Domanski, J.-P. Correa-Baena, M. K. Nazeeruddin, S. M. Zakeeruddin, W. Tress, A. Abate, A. Hagfeldt, M. Gratzel, *Energy Environ. Sci.* **2016**, *9*, 1989.
[23] A. Guerrero, G. Garcia-Belmonte, I. Mora-Sero, J. Bisquert, Y. S. Kang, T. J. Jacobsson, J.-P. Correa-Baena, A. Hagfeldt, *J. Phys. Chem. C* **2016**, *120*, 8023.
[24] a) A. Dualeh, T. Moehl, N. Tétreault, J. Teuscher, P. Gao, M. K. Nazeeruddin, M. Grätzel, *ACS Nano* **2014**, *8*, 362; b) E. J. Juarez-Perez, R. S. Sanchez, L. Badia, G. Garcia-Belmonte, Y. S. Kang, I. Mora-Sero, J. Bisquert, *J. Phys. Chem. Lett.* **2014**, *5*, 2390; c) V. Gonzalez-Pedro, E. J. Juarez-Perez, W.-S. Arsyad, E. M. Barea, F. Fabregat-Santiago, I. Mora-Sero, J. Bisquert, *Nano Lett.* **2014**, *14*, 888; d) B. Suarez, V. Gonzalez-Pedro, T. S. Ripolles, R. S. Sanchez, L. Otero, I. Mora-Sero, *J. Phys. Chem. Lett.* **2014**, *5*, 1628.
[25] T. A. Berhe, W.-N. Su, C.-H. Chen, C.-J. Pan, J.-H. Cheng, H.-M. Chen, M.-C. Tsai, L.-Y. Chen, A. A. Dubale, B.-J. Hwang, *Energy Environ. Sci.* **2016**, *9*, 323.